Spin splitting of electron states in lattice-mismatched (110)-oriented quantum wells

M. O. Nestoklon,[1] S. A. Tarasenko,[1] R. Benchamekh,[2] and P. Voisin[3]
[1]*Ioffe Institute, 194021 St. Petersburg, Russia*
[2]*Tyndall National Institute, Lee Maltings, Dyke Parade, Cork, Ireland*
[3]*Laboratoire de Photonique et Nanostructures, CNRS and Université Paris-Saclay, Route de Nozay, 91460 Marcoussis, France*
(Received 1 June 2016; revised manuscript received 26 August 2016; published 27 September 2016)

We show that for lattice-mismatched zinc-blende-type (110)-grown quantum wells a significant contribution to the zero-magnetic-field spin splitting of electron subbands comes from strain-induced spin-orbit coupling. Combining the envelope function theory and atomistic tight-binding approach, we calculate spin-orbit splitting constants for realistic quantum wells. It is found that the strain due to lattice mismatch in conventional GaAs/AlGaAs structures may noticeably modify the spin splitting while in InGaAs/GaAs structures it plays a major role and may even change the sign of the spin splitting constant.

DOI: 10.1103/PhysRevB.94.115310

I. INTRODUCTION

The $\boldsymbol{k}$-linear spin-orbit splitting of electron states in zinc-blende-type quantum wells (QWs) is usually discussed in terms of the Rashba spin-orbit coupling stemming from structure inversion asymmetry (SIA) [1–3] and the Dresselhaus spin-orbit coupling originating from $\boldsymbol{k}$-cubic terms in the bulk crystal spectrum (also named BIA contribution) [4,5] and interface inversion asymmetry (IIA) [6–10], or their interplay [11–21]. Here, $\boldsymbol{k}$ is the electron wave vector. Although it is well known that all QW structures are strained in a varying degree depending on the lattice mismatch between the QW and the buffer layer and that strain may also give rise to $\boldsymbol{k}$-linear spin-orbit coupling in bulk crystals [22–24], the effect of strain on spin splitting is commonly neglected. This is largely due to the fact that, in the most studied GaAs/AlGaAs heterostructures, the lattice mismatch does not exceed 0.5% and the whole epilayer adopts the GaAs substrate lattice parameter.

Recently, it has been demonstrated experimentally that strain may give a significant contribution to spin splitting in real lattice-mismatched heterostructures [25], but there are a lack of theoretical studies of this effect. The strain caused by lattice mismatch can affect the spin splitting in QWs of any crystallographic orientation. However, this effect is expected to be more pronounced in QWs of any orientation other than (001) since the shear (in cubic axes) strain naturally occurring in low-symmetry heterostructures directly couples the conduction-band and valence-band states [22,23]. Therefore, we focus here on (110)-grown quantum wells. We combine the envelope function theory and advanced atomistic tight-binding calculations and prove that this strain-induced effect can be large as to dominate the spin properties of some lattice-mismatched (110)-grown structures. The tight-binding approach allows us to take into account the effect of local strain determined by the local arrangement of atoms on the band structure as well as interface effects. It is found that the strain-induced spin-orbit coupling is already sizable for a GaAs/AlGaAs QW when the lattice mismatch is supported by the GaAs well. The calculations performed for a InGaAs-based QW yield that the strain is the major source of spin-orbit coupling in the conduction subbands. The resulting Dresselhaus constant of the spin-orbit splitting in InGaAs-based QWs considerably exceeds that in GaAs/AlGaAs structures and, more importantly, can be of different sign depending on the buffer layer used.

II. EFFECTIVE HAMILTONIAN

The effective Hamiltonian describing $\boldsymbol{k}$-linear spin splitting of electron states in a (110)-grown QW may be generally presented as a sum of three contributions [26]

$$H_{so} = \beta\sigma_z k_x + \alpha_+(\sigma_x k_y - \sigma_y k_x) + \alpha_-(\sigma_x k_y + \sigma_y k_x), \quad (1)$$

where σ_j $(j = x,y,z)$ are the Pauli matrices, $x \parallel [1\bar{1}0]$ and $y \parallel [00\bar{1}]$ are the in-plane axes, and $z \parallel [110]$ is the growth axis. The first term on the right-hand side of Eq. (1) is the $\boldsymbol{k}$-linear Dresselhaus term which originates from BIA and IIA. This term will be drastically affected by strain. The second term describes the isotropic Rashba spin-orbit coupling stemming from SIA. The third term emerges if both the atomic structure of the QW interfaces and the QW structure inversion asymmetry are taken into account. Both the second and the third terms vanish in symmetrically grown QWs.

Atomistic tight-binding calculations carried out recently for (110) GaAs/$Al_{0.3}Ga_{0.7}As$ QWs [26] revealed that the values of β and α_+ are in a good agreement with the results of the envelope function calculations and α_-, which is absent in the isotropic Rashba model, is an order of magnitude smaller than α_+. We note that misfit strain was "switched off" in the calculations of Ref. [26] since it is rather weak in GaAs/AlGaAs heterostructures.

The deformation of a bulk zinc-blende-type crystal leads to a $\boldsymbol{k}$-linear spin splitting of the electron spectrum [23]. The corresponding bulk Hamiltonian written in the cubic axes $\tilde{x} \parallel [100]$, $\tilde{y} \parallel [010]$, and $\tilde{z} \parallel [001]$ has the form

$$H_{\rm str} = \tfrac{1}{2}(C_3\,\boldsymbol{\sigma}\cdot\boldsymbol{\varphi} + C_3'\,\boldsymbol{\sigma}\cdot\boldsymbol{\psi}), \quad (2)$$

where C_3 and C_3' are material constants, $\boldsymbol{\varphi}$ and $\boldsymbol{\psi}$ are the pseudovectors constructed from the components of the strain tensor $\boldsymbol{\varepsilon}$ and the wave vector $\boldsymbol{k}$,

$$\boldsymbol{\varphi} = \begin{bmatrix} \varepsilon_{\tilde{x}\tilde{y}}k_{\tilde{y}} - \varepsilon_{\tilde{x}\tilde{z}}k_{\tilde{z}} \\ \varepsilon_{\tilde{y}\tilde{z}}k_{\tilde{z}} - \varepsilon_{\tilde{x}\tilde{y}}k_{\tilde{x}} \\ \varepsilon_{\tilde{x}\tilde{z}}k_{\tilde{x}} - \varepsilon_{\tilde{y}\tilde{z}}k_{\tilde{y}} \end{bmatrix}, \quad \boldsymbol{\psi} = \begin{bmatrix} (\varepsilon_{\tilde{y}\tilde{y}} - \varepsilon_{\tilde{z}\tilde{z}})k_{\tilde{x}} \\ (\varepsilon_{\tilde{z}\tilde{z}} - \varepsilon_{\tilde{x}\tilde{x}})k_{\tilde{y}} \\ (\varepsilon_{\tilde{x}\tilde{x}} - \varepsilon_{\tilde{y}\tilde{y}})k_{\tilde{z}} \end{bmatrix}. \quad (3)$$

In the (xyz) coordinate frame relevant to (110)-grown structures, the scalar products $\boldsymbol{\sigma}\cdot\boldsymbol{\varphi}$ and $\boldsymbol{\sigma}\cdot\boldsymbol{\psi}$ assume the form

$$\begin{aligned}\boldsymbol{\sigma}\cdot\boldsymbol{\varphi} &= \tfrac{1}{2}(\varepsilon_{zz}-\varepsilon_{xx})(\sigma_x k_z-\sigma_z k_x)\\ &\quad -\varepsilon_{xy}(\sigma_y k_x+\sigma_z k_y)-\varepsilon_{yz}(\sigma_x k_y-\sigma_y k_x),\\ \boldsymbol{\sigma}\cdot\boldsymbol{\psi} &= \tfrac{1}{2}(\varepsilon_{xx}-2\varepsilon_{yy}+\varepsilon_{zz})(\sigma_x k_z+\sigma_z k_x)\\ &\quad -\varepsilon_{xz}(\sigma_x k_x-2\sigma_y k_y+\sigma_z k_z).\end{aligned} \tag{4}$$

Lattice mismatch in a (110)-grown structure leads to the emergence of the strain tensor components $\varepsilon_{xx}=\varepsilon_{yy}$ and ε_{zz} while the off-diagonal components (in the QW coordinate frame) do not occur. The strain tensor can be decomposed in two parts: isotropic part which induces only a change of the band positions, effective mass, and the bulk Dresselhaus constant and anisotropic part with the zero trace which gives rise to $\boldsymbol{k}$-linear spin-orbit coupling. Taking into account that electrons are confined in a QW along the z direction, i.e., $\langle k_z\rangle=0$, one obtains the strain-induced contribution to the spin Hamiltonian

$$H_{\rm srt}^{\rm QW}=\tfrac{1}{4}(C_3-C_3')(\varepsilon_{xx}-\varepsilon_{zz})\sigma_z k_x, \tag{5}$$

which corresponds to an additional contribution $\beta_{\rm str}$ to the Dresselhaus constant [see Eq. (1)]

$$\beta_{\rm str}=\tfrac{1}{4}(C_3-C_3')(\varepsilon_{xx}-\varepsilon_{zz}). \tag{6}$$

It is interesting to compare $\beta_{\rm str}$ with the usual Dresselhaus constant β for a standard (110)-grown GaAs/$Al_{0.3}Ga_{0.7}$As QW. The deformation constants for GaAs obtained from the *ab initio* calculations of Ref. [27] are $C_3\sim 4$–8 eV Å and $C_3'\sim 2$ eV Å. Recent experimental estimations give $C_3\approx 8.1$ eV Å and C_3' is negligibly small [28]. The typical values of β are in the range 7–15 meV Å [26] while the lattice mismatch is $\epsilon=\varepsilon_{xx}-\varepsilon_{zz}\sim 1\times 10^{-3}$. Assuming that misfit strain is supported by the GaAs well, we conclude that the strain-induced spin-orbit coupling is only few times smaller than the regular BIA term in such AlGaAs heterostructures.

Conversely, in a $In_{0.2}Ga_{0.8}$As/GaAs QW, where the strain $\epsilon\sim 0.02$ is typically 20 times larger and the deformation constant C_3 is also larger (see below), the strain-induced spin splitting dominates over the other mechanisms.

To conclude this section, we note that in addition to the renormalization of the Dresselhaus term, nonsymmetric strain near interfaces in realistic structures may also produce electric-field-independent contributions to the α_+ and α_- Rashba terms.

III. TIGHT-BINDING CALCULATIONS

To calculate the electron dispersion in a QW and extract the parameters of spin-orbit coupling we use the well-established $sp^3d^5s^*$ tight-binding method [26,29]. The method is described in a number of papers and will not be repeated here. Instead, we focus in this section on the procedure of strain incorporation into tight binding.

We use the standard crystallographic coordinate system with a cation atom located at the origin and one of its neighboring anions located at $(a_0/4,a_0/4,a_0/4)$, with a_0 being the lattice constant. Note that the opposite choice of the coordinate frame leading to the opposite sign of the bulk Dresselhaus constant γ_c and the deformation constant C_3 is also utilized in literature.

The strain is microscopically calculated in the valence force field (VFF) approximation [30] which is able to provide reliable results for small and intermediate strains [31]. To model realistic structures, we set the lateral lattice constant fixed to mimic the lattice-matched growth on a substrate. Then, we keep the lateral periodic boundary conditions fixed and vary the positions of atoms using the conjugate gradient method to minimize the VFF elastic energy. After the minimization, we obtain the atomic positions for the fully relaxed structure. This allows us to extract a microscopic strain tensor acting on atomic orbitals using an approach similar to that described in Ref. [32], as explained below.

For each atom we calculate the "local strain tensor" based on the positions of its four neighboring atoms. For a cation C surrounded with four anions A_i $(i=1\ldots4)$ located at arbitrary positions, the local strain acting on the cation is defined according to the following procedure. First, the nominal anion positions $\boldsymbol{r}_{(0)i}$ are determined from the bond lengths corresponding to the CA_i bulk lattice parameters in the absence of bond bending. After the structure relaxation, this nominal tetrahedron determined by $\boldsymbol{r}_{(0)i}$ transforms into the actual one given by the real positions of the atoms $\boldsymbol{r}_i$. The nominal and actual tetrahedrons can be uniquely characterized by three vectors $\boldsymbol{R}_j$ and $\boldsymbol{R}_{(0)j}$ $(j=1\ldots3)$, respectively. We choose them as follows: $\boldsymbol{R}_{(0)1}=\boldsymbol{r}_{(0)2}-\boldsymbol{r}_{(0)1}$, $\boldsymbol{R}_{(0)2}=\boldsymbol{r}_{(0)4}-\boldsymbol{r}_{(0)3}$, and $\boldsymbol{R}_{(0)3}=[\boldsymbol{r}_{(0)4}+\boldsymbol{r}_{(0)3}-\boldsymbol{r}_{(0)2}-\boldsymbol{r}_{(0)1}]/2$. Then, we calculate the matrix $\boldsymbol{T}$ connecting the nominal and strained sets $\boldsymbol{R}_j=\boldsymbol{T}\boldsymbol{R}_{(0)j}$. The local strain tensor $\boldsymbol{\varepsilon}$ is then defined by the polar decomposition $\boldsymbol{T}=(1+\boldsymbol{\varepsilon})\boldsymbol{R}$, where $\boldsymbol{R}$ is the orthogonal matrix of rotation.

One may check that, for a homogeneously strained bulk binary compound, this approach reproduces the classical definition of strain tensor. However, the approach allows one to generalize the concept of the strain tensor to the atomic scale.

We notice that the tensor $\boldsymbol{\varepsilon}$ does not fully describe the local atomic configuration: It is uniquely defined by the relative coordinates of four anions surrounding a given cation (or, vice versa, by the cation relative coordinates surrounding a given anion) while the change in the cation position does not affect $\boldsymbol{\varepsilon}$. To account for the cation position change, we additionally introduce an internal strain vector $\boldsymbol{u}$ defined as the displacement of the cation from the point equidistant from the surrounding anions and scaled to the unstrained interatomic distance. For homogeneously strained bulk crystal, the strain tensor $\boldsymbol{\varepsilon}$ and the strain vector $\boldsymbol{u}$ are proportional to each other and related by the Kleinman parameter [30]. However, this is not generally the case for equilibrium atom positions in a structure with different chemical bonds.

The local strain tensor $\boldsymbol{\varepsilon}$ and the local strain vector $\boldsymbol{u}$ are then incorporated into the tight-binding Hamiltonian. The strain contribution to the tight-binding Hamiltonian has three rather distinct parts. The first one is a scaling of the transfer matrix elements due to the change in the bond lengths [29]

$$V_{n_1,n_2;ijk}=V^0_{n_1,n_2;ijk}\left(\frac{d_{n_1,n_2}}{d^0_{n_1,n_2}}\right)^{n_{ijk}}, \tag{7}$$

TABLE I. Tight-binding parameters used in calculations.

	InAs	GaAs	AlAs
a	6.0580	5.6500	5.6600
E_s^a	−6.0738	−5.9820	−6.5474
$E_{s^*}^a$	17.2502	19.4477	18.9475
E_s^c	0.2582	−0.3803	0.3883
$E_{s^*}^c$	17.2393	19.4548	18.9438
E_p^a	2.8784	3.3087	2.9314
E_d^a	11.7833	13.2015	12.4961
E_p^c	5.6829	6.3801	5.7735
E_d^c	11.7991	13.2055	12.4992
$ss\sigma$	−1.5096	−1.6874	−1.8436
$s_a^* s_c \sigma$	−2.0155	−2.1059	−1.7884
$s_a s_c^* \sigma$	−1.1496	−1.5212	−1.3059
$s^* s^* \sigma$	−3.3608	−3.7170	−3.6128
$s_a p_c \sigma$	2.2807	2.8846	2.5778
$s_c p_a \sigma$	2.6040	2.8902	2.7962
$s_a^* p_c \sigma$	1.9930	2.5294	2.1581
$s_c^* p_a \sigma$	2.0708	2.3883	2.2397
$s_a d_c \sigma$	−2.8945	−2.8716	−2.5624
$s_c d_a \sigma$	−2.3175	−2.2801	−2.3841
$s_a^* d_c \sigma$	−0.6393	−0.6568	−0.8046
$s_c^* d_a \sigma$	−0.5949	−0.6113	−0.7492
$pp\sigma$	3.6327	4.4048	4.1971
$pp\pi$	−0.9522	−1.4471	−1.3146
$p_a d_c \sigma$	−1.1156	−1.6035	−1.6473
$p_c d_a \sigma$	−1.3426	−1.6260	−1.7603
$p_a d_c \pi$	1.2101	1.8423	1.7647
$p_c d_a \pi$	1.5282	2.1421	2.1100
$dd\sigma$	−0.8381	−1.0885	−1.2241
$dd\pi$	1.9105	2.1560	2.1770
$dd\delta$	−1.3348	−1.8607	−1.7585
$\Delta_a/3$	0.1558	0.1745	0.1721
$\Delta_c/3$	0.1143	0.0408	0.0072

where n_1 and n_2 are the indices denoting two neighboring atoms, ijk encodes the corresponding Slater off-diagonal parameter, $V^0_{n_1,n_2;ijk}$ is the transfer matrix element in the unstrained bulk binary compound, d_{n_1,n_2} and $d^0_{n_1,n_2}$ are the relaxed interatomic distance and the chemical bond length in the corresponding unstrained compound, and n_{ijk} is the power-law scaling exponent [29]. For calculations here we use a set of tight-binding parameters listed in Table I.

The second contribution, also introduced in Ref. [29], is the shift of onsite energies proportional to the hydrostatic component of strain,

$$\delta E_\beta = E_\beta - E^0_\beta = -\alpha_\beta \left(E^0_\beta - E_{\rm ref}\right)\frac{{\rm Tr}\,\varepsilon}{3}, \tag{8}$$

where E^0_β are the onsite energies in the absence of strain (Table I), α_β are the deformation parameters given in Table II, and the index β enumerates the orbitals. We define the energy shifts with respect to the reference energy $E_{\rm ref} = E_{s^*} - 6E_{\langle 1,0,0\rangle}$, where $E_{\langle 1,0,0\rangle} = \hbar^2(2\pi/a)^2/2m_0$ and a is the lattice constant. The introduction of $E_{\rm ref}$ in Eq. (8) allows us to avoid the recalculation of the deformation parameter α_β for heterostructures with band offsets. The present gauge-invariant formulation is, in the linear limit, strictly equivalent to the one used in Refs. [29,33] for the free-electron crystal. The choice

TABLE II. Deformation tight-binding parameters used in calculations. Other parameters are $\alpha_{s^*} = 2.0$ and $n_{s^*s^*\sigma} = n_{s^*d\sigma} = n_{dd\sigma} = n_{dd\pi} = n_{dd\delta} = 2.0$.

	InAs	GaAs	AlAs
α_s^a	0.5603	0.0000	0.9720
α_p^a	1.9539	1.6257	1.8880
α_d^a	1.7005	2.4531	2.0600
α_s^c	0.5603	0.0000	0.9720
α_p^c	1.9539	1.6257	1.8880
α_d^c	1.7005	2.4531	2.0600
$n_{ss\sigma}$	5.4002	4.5619	2.0880
$n_{sp\sigma}$	4.4014	3.0363	5.7560
$n_{sd\sigma}$	6.8053	3.1594	4.4720
$n_{ss^*\sigma}$	5.8401	3.2676	2.8600
$n_{s^*p\sigma}$	6.8116	6.9229	3.2240
$n_{pp\sigma}$	6.9787	6.2602	5.1560
$n_{pp\pi}$	6.0189	7.0824	2.7960
$n_{pd\sigma}$	2.7559	3.5344	5.5920
$n_{pd\pi}$	6.0212	7.3976	4.8080
π_{001}	0.0952	0.1476	0.1000
π_{111}	0.1456	0.1588	0.1160

made for the reference energy is motivated by the aim to keep the positions of the s^* orbitals the same as in the free-electron approximation.

The third contribution is related to the strain-induced splitting of the onsite energies of the degenerate orbitals p and d [33–36]. The contribution has not been analyzed in detail so far. In Ref. [33], a simplified approach has been considered: the splittings were assumed to be proportional to the strain tensor. Here, we generalize this approach by introducing the corrections proportional to the local strain tensor $\boldsymbol{\varepsilon}$ and the local strain vector $\boldsymbol{u}$.

Using the method of invariants one can show that the corresponding contribution to the p-orbital same-atom block in the tight-binding Hamiltonian in the basis of the functions p_x, p_y, and p_z has the form

$$\delta H = \begin{pmatrix} \lambda_1(\sqrt{3}\varepsilon_1 - \varepsilon_2) & \lambda_2\varepsilon_{xy} + \xi u_z & \lambda_2\varepsilon_{zx} + \xi u_y \\ \lambda_2\varepsilon_{xy} + \xi u_z & -\lambda_1(\sqrt{3}\varepsilon_1 + \varepsilon_2) & \lambda_2\varepsilon_{yz} + \xi u_x \\ \lambda_2\varepsilon_{zx} + \xi u_y & \lambda_2\varepsilon_{yz} + \xi u_x & 2\lambda_1\varepsilon_2 \end{pmatrix}, \tag{9}$$

where $\varepsilon_1 = \sqrt{3}(\varepsilon_{xx} - \varepsilon_{yy})$, $\varepsilon_2 = 2\varepsilon_{zz} - \varepsilon_{xx} - \varepsilon_{yy}$, and λ_j $(j = 1,2)$ are parameters, and we assume $\xi = \pm\lambda_2$ for anions and cations, respectively. To make the parametrization space more compact, we assume that the parameters λ_j for anions and cations are connected to each other by

$$\begin{aligned} \lambda_1^a &= \tfrac{1}{2}\left(E_p^a - E_{\rm ref}^a\right)\pi_{100},\ \lambda_1^c = \tfrac{1}{2}\left(E_p^c - E_{\rm ref}^c\right)\pi_{100}, \\ \lambda_2^a &= -\tfrac{8}{3}\left(E_p^a - E_{\rm ref}^a\right)\pi_{111},\ \lambda_2^c = -\tfrac{8}{3}\left(E_p^c - E_{\rm ref}^c\right)\pi_{111}. \end{aligned} \tag{10}$$

The deformation parameters π_{100} and π_{111} for several binary compounds are listed in Table II. We note that similar splitting occurs for the d orbitals as well. However, to fit the conduction-band and valence-band deformation-potential constants at the Γ point of the Brillouin zone it is sufficient to consider the splitting of the p orbitals. Therefore, to simplify calculations, we neglect the splitting of the d orbitals. We keep in mind that

TABLE III. The band gaps E_g (in eV), the effective electron masses at the Γ point m_e (in the units of free-electron mass), the bulk Dresselhaus constants γ_c (in eV Å^3) (see footnote 1), the deformation-potential constants a_c, a_v, b, and d (in eV), and C_3 (in eV Å) computed using the tight-binding parameters from Tables I and II.

	GaAs	AlAs	InAs	$Al_{0.3}Ga_{0.7}As$	$In_{0.2}Ga_{0.8}As$
E_g	1.519	3.130	0.417	2.000	1.207
m_e	0.0665	0.158	0.0235	0.0904	0.0519
$-\gamma_c$	24.21	9.12	45.39	16.04	28.61
a_c	−7.17	−5.64	−5.08	−6.74	−6.62
a_v	1.60	2.47	1.00	1.63	1.22
b	−2.00	−2.30	−1.80	−0.74	−1.35
d	−4.80	−3.40	−3.60	−4.39	−4.53
$-C_3$	8.12	−3.34	104.5	−2.65	15.10

for fitting simultaneously the deformation-potential constants at the Γ, X, and L points a complete set of parameters should be used.

The determination of the strain-related parameters of the tight-binding Hamiltonian is a challenging task because of the small number of available well-documented deformation-potential constants. In fact, the deformation-potential constants at the Brillouin zone center do not provide enough information to uniquely determine all the tight-binding parameters. We expect that any parametrization providing the correct values of the conduction-band deformation-potential constant a_c and the valence-band deformation-potential constants a_v, b, and d yields satisfactory results for the strain-induced spin-orbit coupling. Therefore, we adopt the approach described in Ref. [37] and numerically fit the strain-related tight-binding parameters to reproduce the recommended values of the deformation-potential constants in the Brillouin zone center given in Ref. [38]. The obtained parameters are presented in Table II. Table III summarizes the band gaps E_g, the effective electron masses at the Γ point m_e, the Dresselhaus constants γ_c, and the deformation-potential constants a_c, a_v, b, d, and C_3 for some bulk binary and ternary compounds obtained from the tight-binding calculations with the parameters listed in Tables I and II.

For alloys, the tight-binding needs a special care to be taken to reproduce the band-gap bowing properly [39]. Here, we use an original interpolation scheme [40] to construct the alloy $A_xB_{1-x}C$ tight-binding parameters in the virtual crystal approximation from the tight-binding parameters of the binary compounds AC and BC. First, the lattice constant of the alloy is found as the linear interpolation between the binaries. Then, we calculate the strain contributions as described above and construct the parameters of the AC and BC materials strained to the lattice constant of the alloy. Finally, the tight-binding parameters of the alloy are determined as the linear interpolations of the parameters of the strained binary materials. We note that, unlike the approach from Ref. [39], this procedure provides the correct bowing without the introduction of additional parameters.

We also note that the standard $sp^3d^5s^*$ tight-binding model [29] does not take into account the spin-orbit coupling of the p and d orbitals which yields the major contribution

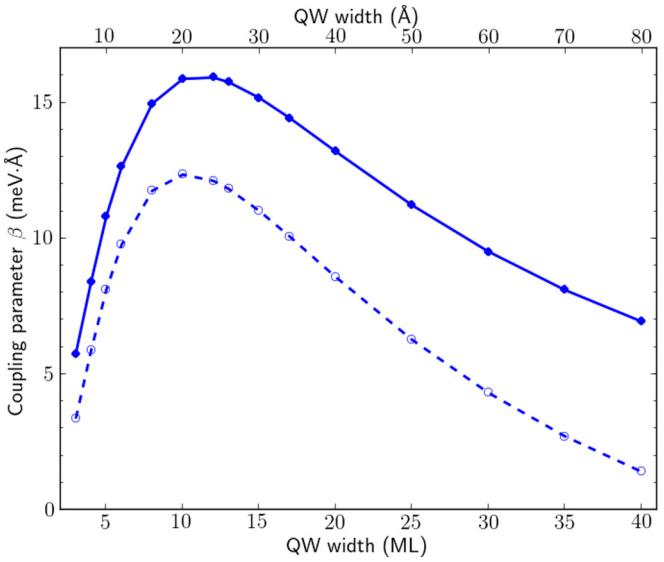

FIG. 1. Dresselhaus constant β as a function of the QW thickness (in monolayers, ML) calculated for $Al_{0.3}Ga_{0.7}As/GaAs/Al_{0.3}Ga_{0.7}As$ QWs with different strain configurations. Solid line shows the results for QW structures with the lattice constant corresponding to GaAs, $a_0 = 5.65$ Å (the barrier strain $\epsilon = -8.6 \times 10^{-4}$). Dashed line shows the results for QWs lattice matched to AlAs with the lattice constant $a_0 = 5.66$ (the QW strain $\epsilon = 2.0 \times 10^{-3}$, the barrier strain $\epsilon = 2.9 \times 10^{-3}$).

to the C_3' constant [23]. The missing of C_3' has the same origin as the missing of the $\boldsymbol{k}$-linear spin splitting of the Γ_8 valence band in the bulk crystal [23,41]. Possible solution of this problem proposed by Boykin [41] is based on the consideration of second-nearest-neighbor tight-binding model with the nearest-neighbor spin-orbit interaction and has no straightforward extension to strained heterostructures.

IV. RESULTS

We use the procedure described in Ref. [26] to extract the constants of the spin-orbit Hamiltonian (1) from the tight-binding calculations for GaAs-based and InGaAs-based QW structures. As distinct from previous calculations, we now include the atomistic strain as described in Sec. III. The results show that the constants $\alpha_\pm$ related to structure inversion asymmetry are almost independent of the strain present in the QW. Therefore, we focus below on the Dresselhaus parameter β and consider symmetric QWs.

A. GaAs/AlGaAs quantum wells

The Dresselhaus constant β as a function of the QW thickness determined for AlGaAs/GaAs/AlGaAs QWs with different strain configurations is shown in Fig. 1. Here, we present the results for the same structures but lattice-matched either to GaAs (solid line) or to AlAs (dashed line).[1] The observed dependencies of β on the QW thickness

[1]The coordinate system is changed with respect to the one used in Ref. [26] which results in the opposite sign of the Dresselhaus constant.

are nonmonotonic. This is expected for the splitting mainly originating from the $\boldsymbol{k}$-cubic terms in the host bulk crystals and actually reflects the strength of electron quantum confinement [5,26]. The energy of size quantization is small in narrow or wide QWs, where electrons reside mostly in the barriers or in the well, respectively, and reaches a maximum for the QW of an intermediate thickness.

From Fig. 1 one may conclude that the widely adopted consideration of GaAs/AlGaAs heterostructures as unstrained systems is not completely satisfied for the analysis of spin splitting. The ratio of the Dresselhaus constants β for the structures lattice matched to GaAs and AlAs would exceed a factor 2 for a 50-Å-wide QW while the strain itself is only 2×10^{-3}. Despite the fact that spin splitting in GaAs/AlGaAs structures is rather small, the spin splitting constants are among the most important parameters of QWs since they determine the spin dynamics and the spin lifetime of electrons [5,19–21].

B. InGaAs/GaAs quantum wells

While the strain contribution to the spin splitting in GaAs/AlGaAs QWs is still a correction, it is natural to expect that in heterostructures grown from compounds with a significant lattice mismatch, like InGaAs/GaAs QWs, the strain contribution dominates the spin splitting.

In addition to larger lattice mismatch, the deformation constant C_3 in InAs is about an order of magnitude larger than that in GaAs (see Table III). The large value of C_3 can be explained from the $\boldsymbol{k} \cdot \boldsymbol{p}$ perturbation theory for bulk crystals where the major contribution to C_3 is given by [23]

$$C_3 = \frac{4}{3} \frac{C_2 P \Delta}{E_g (E_g + \Delta)}, \tag{11}$$

where C_2 is the interband deformation-potential constant, P is the Kane matrix element, and Δ is the spin-orbit splitting of the valence band. The growth of C_3 for InAs as compared to that for GaAs is caused by the decrease in E_g and the increase in C_2.

To elaborate this expectation, we calculate the Dresselhaus constant β for GaAs/$In_{0.2}Ga_{0.8}As$/GaAs QW structures lattice matched to GaAs and $In_{0.2}Ga_{0.8}As$. The dependence of the Dresselhaus constants on the QW thickness for both strain configurations is shown in Fig. 2. The range of spin splittings is significantly larger than that in GaAs/AlGaAs structures and the Dresselhaus constant has a different dependence on the QW thickness. Importantly, the sign of β is opposite for the QW structures lattice matched to GaAs and InGaAs layers. In the first case, β tends to zero for narrow wells and saturates to the constant β_{srt} of the strained bulk InGaAs layer for wide wells (dashed-dotted line). Note that hydrostatic strain may also renormalize the C_3 constant. In the latter case, the behavior is opposite: β tends to the constant β_{srt} of the strained bulk GaAs layer for narrow wells and vanishes for wide wells. The effect of quantum confinement given by $\langle k_z^2 \rangle$, which is important for GaAlAs QWs, is masked by the interplay between the strain and the electron probability of presence in the well and the barriers. Actually, the expected positive value of β for thick unstrained wells (dashed line in Fig. 2) is recovered only for very large thicknesses (>60 ML).

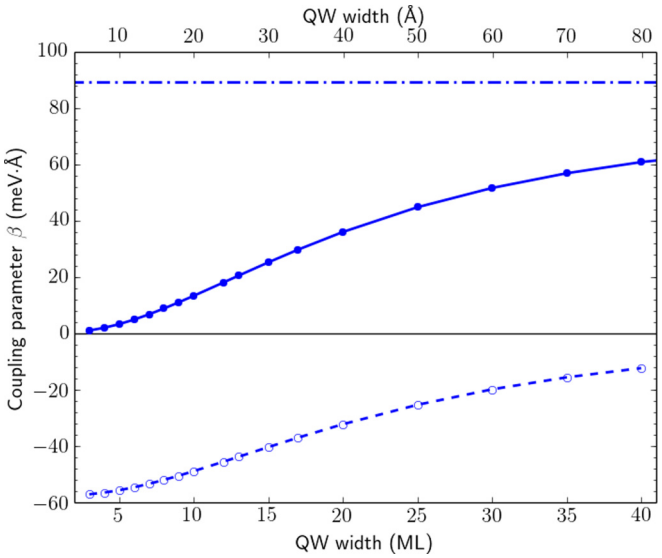

FIG. 2. Dresselhaus constant β as a function of the QW thickness calculated for GaAs/$In_{0.2}Ga_{0.8}As$/GaAs QWs with different strain configurations. Solid and dashed lines show the results for QW structures grown on GaAs buffer layer (the QW strain $\epsilon = -0.024$) and $In_{0.2}Ga_{0.8}As$ buffer layer (the barrier strain $\epsilon = 0.024$), respectively. Dashed-dotted line shows the constant of linear spin splitting in bulk (110)-grown $In_{0.2}Ga_{0.8}As$ alloy with $\epsilon = -0.024$ and C_3 from Table III.

V. CONCLUSION

In conclusion, we have performed atomistic calculations of the spin-orbit splitting of electron subbands in III-V (110)-grown quantum wells and revealed the important role of strain which naturally occurs in heterostructures. The strain contribution to the spin-orbit coupling noticeably renormalizes the Dresselhaus constant in GaAs/AlGaAs QWs, which are commonly treated as nearly unstrained, and dominates the spin splitting in InGaAs/GaAs QWs with a rather large lattice constant mismatch. Strain engineering thus opens a way to control the spin splittings in two-dimensional electron gas in semiconductor heterostructures.

ACKNOWLEDGMENTS

This work was supported by the Russian-French International Laboratory ILNACS, the Russian Foundation for Basic Research (RFBR) (Projects No. 14-02-00123 and No. 15-32-20828), and the European Union 7th Framework Programme DEEPEN (Grant Agreement No. 604416).

[1] F. T. Vasko and N. A. Prima, Fiz. Tverd. Tela **21**, 1734 (1979) [Sov. Phys.–Solid State **21**, 994 (1979)].

[2] Y. A. Bychkov and E. Rashba, Pis'ma Zh. Eksp. Teor. Fiz. **39**, 66 (1984) [JETP Lett. **39**, 78 (1984)].

[3] E. Y. Sherman, Appl. Phys. Lett. **82**, 209 (2003).
[4] G. Dresselhaus, Phys. Rev. **100**, 580 (1955).
[5] M. I. D'yakonov and V. Y. Kachorovskii, Fiz. Tekh. Poluprovodn. **20**, 178 (1986) [Sov. Phys.–Semicond. **20**, 110 (1986)].
[6] E. L. Ivchenko, A. Y. Kaminski, and U. Rössler, Phys. Rev. B **54**, 5852 (1996).
[7] O. Krebs, D. Rondi, J. L. Gentner, L. Goldstein, and P. Voisin, Phys. Rev. Lett. **80**, 5770 (1998).
[8] L. Vervoort, R. Ferreira, and P. Voisin, Semicond. Sci. Technol. **14**, 227 (1999).
[9] M. O. Nestoklon, L. E. Golub, and E. L. Ivchenko, Phys. Rev. B **73**, 235334 (2006).
[10] S. A. Tarasenko, M. V. Durnev, M. O. Nestoklon, E. L. Ivchenko, J.-W. Luo, and A. Zunger, Phys. Rev. B **91**, 081302 (2015).
[11] W. Zawadzki and P. Pfeffer, Semicond. Sci. Technol. **19**, R1 (2004).
[12] X. Cartoixà, L.-W. Wang, D. Z.-Y. Ting, and Y.-C. Chang, Phys. Rev. B **73**, 205341 (2006).
[13] M. O. Nestoklon, E. L. Ivchenko, J.-M. Jancu, and P. Voisin, Phys. Rev. B **77**, 155328 (2008).
[14] R. Winkler, L. Wang, Y. Lin, and C. Chu, Solid State Commun. **152**, 2096 (2012).
[15] P. Alexeev, Pis'ma Zh. Eksp. Teor. Fiz. **98**, 92 (2013) [JETP Lett. **98**, 84 (2013)].
[16] Z. Devizorova and V. Volkov, Pis'ma Zh. Eksp. Teor. Fiz. **110**, 110 (2013) [JETP Lett. **98**, 101 (2013)].
[17] Z. Devizorova, A. Shchepetilnikov, Y. Nefyodov, V. Volkov, and I. V. Kukushkin, Pis'ma Zh. Eksp. Teor. Fiz. **100**, 111 (2014) [JETP Lett. **102**, 102 (2014)].
[18] V. V. Bel'kov, P. Olbrich, S. A. Tarasenko, D. Schuh, W. Wegscheider, T. Korn, C. Schüller, D. Weiss, W. Prettl, and S. D. Ganichev, Phys. Rev. Lett. **100**, 176806 (2008).
[19] S. A. Tarasenko, Phys. Rev. B **80**, 165317 (2009).
[20] R. Völkl, M. Griesbeck, S. A. Tarasenko, D. Schuh, W. Wegscheider, C. Schüller, and T. Korn, Phys. Rev. B **83**, 241306 (2011).
[21] A. V. Poshakinskiy and S. A. Tarasenko, Phys. Rev. B **87**, 235301 (2013).
[22] G. E. Pikus and A. Titkov, in *Optical Orientation*, edited by F. Mayer and B. Zakharchenya (North Holland, Amsterdam, 1984).
[23] G. E. Pikus, V. A. Maruschak, and A. N. Titkov, Fiz. Tekh. Poluprovodn. **22**, 185 (1988) [Sov. Phys. Semicond. **22**, 115 (1988)].
[24] M. Cardona, N. E. Christensen, and G. Fasol, Phys. Rev. B **38**, 1806 (1988).
[25] T. Matsuda and K. Yoh, J. Cryst. Growth **323**, 52 (2011).
[26] M. O. Nestoklon, S. A. Tarasenko, J.-M. Jancu, and P. Voisin, Phys. Rev. B **85**, 205307 (2012).
[27] A. N. Chantis, M. Cardona, N. E. Christensen, D. L. Smith, M. van Schilfgaarde, T. Kotani, A. Svane, and R. C. Albers, Phys. Rev. B **78**, 075208 (2008).
[28] M. Beck, C. Metzner, S. Malzer, and G. H. Döhler, Europhys. Lett. **75**, 597 (2006).
[29] J.-M. Jancu, R. Scholz, F. Beltram, and F. Bassani, Phys. Rev. B **57**, 6493 (1998).
[30] P. N. Keating, Phys. Rev. **145**, 637 (1966).
[31] S. Steiger, M. Salmani-Jelodar, D. Areshkin, A. Paul, T. Kubis, M. Povolotskyi, H.-H. Park, and G. Klimeck, Phys. Rev. B **84**, 155204 (2011).
[32] C. Pryor, J. Kim, L. W. Wang, A. J. Williamson, and A. Zunger, J. Appl. Phys. **83**, 2548 (1998).
[33] J.-M. Jancu and P. Voisin, Phys. Rev. B **76**, 115202 (2007).
[34] T. B. Boykin, M. Luisier, M. Salmani-Jelodar, and G. Klimeck, Phys. Rev. B **81**, 125202 (2010).
[35] Y. M. Niquet, D. Rideau, C. Tavernier, H. Jaouen, and X. Blase, Phys. Rev. B **79**, 245201 (2009).
[36] M. Zieliński, Phys. Rev. B **86**, 115424 (2012).
[37] F. Raouafi, R. Benchamekh, M. O. Nestoklon, J.-M. Jancu, and P. Voisin, J. Phys.: Condens. Matter **28**, 045001 (2016).
[38] I. Vurgaftman, J. R. Meyer, and L. R. Ram-Mohan, J. Appl. Phys. **89**, 5815 (2001).
[39] K. Shim and H. Rabitz, Phys. Rev. B **57**, 12874 (1998).
[40] M. Nestoklon, R. Benchamekh, and P. Voisin, J. Phys.: Condens. Matter **28**, 305801 (2016).
[41] T. B. Boykin, Phys. Rev. B **57**, 1620 (1998).